

1 This paper was submitted to the Journal of Geophysical Research
2 (We have change a Title; former Title was “Are Ring Current Ions Lost in
3 Dispersion Relation of Electromagnetic Ion Cyclotron Waves?”)

4

5 **Impact of Ring Current Ions on Electromagnetic Ion Cyclotron**
6 **Wave Dispersion Relation**

7 G. V. Khazanov

8 NASA, Marshall Space Flight Center, Huntsville, Alabama, USA

9 K. V. Gamayunov

10 NASA, Marshall Space Flight Center, Huntsville, Alabama, USA

11 Short title: RC ROLE IN EMIC WAVE DISPERSION RELATION

12 **Abstract.** Effect of the ring current ions in the real part of electromagnetic ion
 13 cyclotron wave dispersion relation is studied on global scale. Recent Cluster observations
 14 by *Engebretson et al.* [2007] showed that although the temperature anisotropy of
 15 energetic (> 10 keV) ring current protons was high during the entire 22 November 2003
 16 perigee pass, electromagnetic ion cyclotron waves were observed only in conjunction with
 17 intensification of the ion fluxes below 1 keV by over an order of magnitude. To study the
 18 effect of the ring current ions on the wave dispersive properties and the corresponding
 19 global wave redistribution, we use a self-consistent model of interacting ring current
 20 and electromagnetic ion cyclotron waves [*Khazanov et al.*, 2006], and simulate the
 21 May 1998 storm. The main findings of our simulation can be summarized as follows:
 22 First, the plasma density enhancement in the night MLT sector during the main and
 23 recovery storm phases is mostly caused by injection of suprathermal plasma sheet H^+
 24 ($\lesssim 1$ keV), which dominate the thermal plasma density. Second, during the recovery
 25 storm phases, the ring current modification of the wave dispersion relation leads to a
 26 qualitative change of the wave patterns in the postmidnight–dawn sector for $L > 4.75$.
 27 This “new” wave activity is well organized by outward edges of dense suprathermal ring
 28 current spots, and the waves are not observed if the ring current ions are not included in
 29 the real part of dispersion relation. Third, the most intense wave-induced ring current
 30 precipitation is located in the night MLT sector and caused by modification of the wave
 31 dispersion relation. The strongest precipitating fluxes of about $8 \cdot 10^6$ ($\text{cm}^2 \cdot \text{s} \cdot \text{sr}$)⁻¹
 32 are found near $L=5.75$, $\text{MLT}=2$ during the early recovery phase on 4 May. Finally, the
 33 nightside precipitation is more intense than the dayside fluxes, even if there are less

34 intense waves, because the convection field moves ring current ions into the loss cone on
35 the nightside, but drives them out of the loss cone on the dayside. So convection and
36 wave scattering reinforce each other in the nightside, but interfere in the dayside sector.

1. Introduction

Electromagnetic ion cyclotron (EMIC) waves are a common feature of the Earth magnetosphere. These waves were observed in the inner [e. g., *LaBelle et al.*, 1988; *Erlandson and Ukhorskiy*, 2001] and outer [*Anderson et al.*, 1992a, b] magnetosphere, at geostationary orbit [*Young et al.*, 1981; *Mauk*, 1982], at high latitudes along the plasmopause [*Erlandson et al.*, 1990], and at ionospheric altitudes [*Iyemori and Hayashi*, 1989; *Bräysy et al.*, 1998]. Interaction of the ring current (RC) with EMIC waves causes scattering of ions into the loss cone and leads to decay of the RC [*Cornwall et al.*, 1970]. This wave-induced RC precipitation was studied widely both experimentally and theoretically [e. g., *Soraas et al.*, 1999; *Erlandson and Ukhorskiy*, 2001; *Yahnina et al.*, 2003; *Walt and Voss*, 2001, 2004; *Jordanova et al.*, 2001; *Khazanov et al.*, 2002], which produce RC decay times of about one hour or less during the main phase of storms [*Gonzalez et al.*, 1989]. Obliquely propagating EMIC waves damp due to Landau resonance with thermal plasmaspheric electrons, and cyclotron resonances with thermal, suprathreshold, and hot heavy ions [e. g., *Cornwall et al.*, 1971; *Anderson and Fuselier*, 1994; *Horne and Thorne*, 1997; *Thorne and Horne*, 1994; 1997]. Subsequent transport of the dissipating wave energy into the ionosphere causes ionosphere temperature enhancements [e. g., *Gurgiolo et al.*, 2005]. *Cornwall et al.* [1971] employed the mechanism of resonant energy transfer to electrons to explain stable auroral red arc emissions during the recovery phase of storms. Measurements taken aboard the Prognoz satellites revealed a “hot zone” near the plasmopause where

58 the temperature of core plasma ions can reach tens of thousands of degrees [*Bezrukikh*
59 *and Gringauz*, 1976; *Gringauz*, 1983; 1985]. The earliest results regarding the heating
60 of the cold ions were obtained by *Galeev* [1975] who considered the induced scattering
61 of EMIC waves by plasmaspheric protons as an ion heating mechanism. This nonlinear
62 wave-particle interaction process was used in a plasmasphere-RC interaction model by
63 *Gorbachev et al.* [1992]. Later, a detailed analysis of thermal ion heating by EMIC
64 waves was presented by *Anderson and Fuselier* [1994] and *Fuselier and Anderson*
65 [1996]. Relativistic electrons (≥ 1 MeV) in the outer radiation belt can also interact
66 with EMIC waves [*Thorne and Kennel*, 1971; *Lyons and Thorne*, 1972]. Recently,
67 data from balloon-borne X-ray instruments provided indirect but strong evidence for
68 EMIC wave-induced precipitation of outer-zone relativistic electrons [*Foat et al.*, 1998;
69 *Lorentzen et al.*, 2000]. These observations stimulated theoretical and statistical studies
70 [*Summers and Thorne*, 2003; *Albert*, 2003; *Meredith et al.*, 2003; *Loto'aniu et al.*, 2006]
71 which demonstrated that EMIC wave-induced pitch-angle diffusion of MeV electrons
72 can operate in the strong diffusion limit with a time scale of several hours to a day,
73 and that this mechanism can compete with relativistic electron depletion caused by the
74 adiabatic effect of *Dst* during the initial and main phases of a storm. Therefore, EMIC
75 waves interact well with both the magnetospheric electrons and ions, and these waves
76 are strongly influence the particle dynamics in the eV-MeV energy range.

77 In a number of magnetospheric regimes, a source of free energy for the excitation
78 of EMIC waves is the temperature anisotropy ($T_{\perp} > T_{\parallel}$) of the hot H^+ distribution
79 [*Cornwall*, 1964, 1965; *Kennel and Petschek*, 1966]. Our understanding of EMIC

80 wave growth and propagation was dramatically changed after measurements on board
81 the GEOS 1 and 2 satellites. They revealed the critical role of the thermal He^+ for
82 generation and propagation of EMIC waves [Young *et al.*, 1981; Roux *et al.*, 1982]. The
83 observations stimulated theoretical studies in which the influence of thermal He^+ and
84 O^+ admixtures on EMIC wave properties was considered [Mauk, 1982; Roux *et al.*,
85 1982; Rauch and Roux, 1982; Gomberoff and Neira 1983; Gendrin *et al.*, 1984; Denton
86 *et al.*, 1992; Horne and Thorne, 1993]. The effects of energetic RC heavy ions (He^+
87 and O^+) on the generation of EMIC waves in a multi-ion core plasma (H^+ , He^+ , O^+)
88 were studied by Kozyra *et al.* [1984]. Horne and Thorne [1993] used the “HOTRAY”
89 ray tracing program to study the role of propagation and refraction in the generation of
90 different branches of EMIC waves in a multi-ion thermal plasma. They found that the
91 local growth rate alone cannot determine the resulting wave amplification; propagation
92 effects have a major impact on the path-integrated wave gain, and consequently the
93 prevalent He^+ -mode grows preferably at the plasmopause. Recently, Loto’aniu *et al.*
94 [2005] used magnetic and electric field data from the Combined Release and Radiation
95 Effects Satellite to obtain the Poynting vector for Pc 1 EMIC waves. They found
96 bidirectional wave energy propagation, both away and toward the equator, for events
97 observed below 11° |MLAT|, but unidirectional energy propagation away from the
98 equator for events outside $\pm 11^\circ$ of the equator. Engebretson *et al.* [2005] found a similar
99 EMIC wave energy propagation dependence, with mixed direction within approximately
100 $\pm 20^\circ$ MLAT, but consistently toward the ionosphere for higher magnetic latitudes.
101 These observations allowed Engebretson *et al.* [2007] to state that “the mixed directions

102 observed in the above studies near the equator is evidence of wave reflection at the
103 off-equatorial magnetic latitude corresponding to the ion-ion hybrid frequency. Waves
104 that reflect would then set up a standing (bi-directional) pattern in the equatorial
105 magnetosphere. Waves that tunnel through would tend to be absorbed in the ionosphere
106 and not be able to return to equatorial latitudes.”

107 Starting from the pioneering work of *Kennel and Petschek* [1966], it is well-known
108 that the plasma density is one of the most important plasma characteristics controlling
109 EMIC wave generation; the minimum energy of resonant ions is proportional to the
110 magnetic field energy per particle. In an electron-proton plasma, *Cornwall et al.* [1970]
111 found that the EMIC wave growth rate maximizes just inside the plasmopause where
112 the Alfvén speed is low, falling to zero with both decreasing (because of electron-ion
113 collisions) and increasing L-shell (because of high critical anisotropy). In the case
114 of a multi-ion magnetosphere, *Horne and Thorne* [1993] reported a result opposite
115 to that found by *Cornwall et al.* [1970], namely, the growth rates are substantially
116 greater outside the plasmopause than just inside the plasmopause. The latter is an
117 effect of heavy ions, and both the above results were reconciled by *Kozyra et al.*
118 [1984]. However, *Horne and Thorne* [1993] illustrated that when propagation effects
119 are properly included, the path-integrated wave gain is indeed larger just inside the
120 plasmopause. The effect of the plasmopause in EMIC wave generation is very clearly
121 observed both in experiments [e. g., *Fraser and Nguyen*, 2001], and in the results of
122 numerical simulation [*Kozyra et al.*, 1997; *Khazanov et al.*, 2006]. (Of course, the real
123 magnetospheric situation is more complex, and wave occurrence actually increases with

124 L-shell, which depending on MLT, exhibits a radial structure with a gap between high
125 and low L-shell events [*Anderson et al.*, 1992a].)

126 Recently, *Engbretson et al.* [2007] presented the Cluster observations of EMIC
127 waves in the Pc 1–2 frequency range and associated ion distributions during the October
128 and November 2003 storms. The most intense waves were observed on 22 November
129 near the end of the rapid recovery phase in the dawn MLT sector at L=4.4–4.6.
130 Generation of these waves was associated with anisotropic RC H^+ of energies greater
131 than 10 keV. Although the temperature anisotropy of these energetic protons was high
132 during the entire 22 November event, EMIC waves were observed only in conjunction
133 with intensification of the ion fluxes below 1 keV by over an order of magnitude. This
134 suggests that a suprathermal plasma plays an important role in the destabilization of
135 the more energetic RC and/or plasma sheet ions, because high energy anisotropic RC
136 and/or plasma sheet proton distributions appeared to be a necessary but not sufficient
137 condition for the occurrence of EMIC waves. Similarly, studying Pc 1–2 events in the
138 dayside outer magnetosphere, *Engbretson et al.* [2002] and *Arnoldy et al.* [2005] found
139 that greatly increased fluxes of low energy protons are crucial for the destabilization of
140 the anisotropic RC protons. Those observations provide clear evidence that both the
141 cold plasmaspheric plasma (and, of course, heavy ion content) and the suprathermal
142 ($\lesssim 1$ keV) ions injected from the plasma sheet (and/or ion outflow from the ionosphere)
143 control EMIC wave excitation in the RC. On the other hand, an assumption that the
144 total plasma density/composition is dominated by the thermal plasma was made in
145 previous RC–EMIC wave modeling efforts, and RC ions were not included in the real

146 part of the wave dispersion relation [Kozyra *et al.*, 1997; Jordanova *et al.*, 1998b, 2001;
147 Khazanov *et al.*, 2006], but only in the EMIC wave growth rate. As a result, EMIC waves
148 are only generated near the plasmopause in all these theoretical models. Consequently
149 we generalize our previous self-consistent RC-EMIC wave model [Khazanov *et al.*, 2006]
150 to take into account the effect of RC ions in the real part of the EMIC wave dispersion
151 relation.

152 The present study further develops a self-consistent theoretical model of RC and
153 propagating EMIC waves in a multi-ion magnetospheric plasma [Khazanov *et al.*, 2006],
154 where we take into account the RC ions in the real part of dispersion relation for the
155 He^+ -mode. This article is organized as follows: In section 2 we provide the system of
156 equations which govern our global theoretical model, as well as the initial/boundary
157 conditions used in the simulation of the May 1998 storm; In section 3 we present both
158 the spatial distribution of the total plasma density (thermal + higher energies) during
159 the May 1998 event, and the fine energy structure of the RC phase space distribution
160 functions; In section 4, the effect of plasma density on the EMIC wave growth is
161 illustrated; In section 5, role of the RC ion thermal effects in the He^+ -mode dispersion
162 relation is analyzed; In section 6, results of simulation are presented; Finally, in section 7
163 we summarize the new features of the model, and the findings of the paper.

164 2. Equations of Global Model, Approaches and

165 Initial/Boundary Conditions

For RC species H^+ , O^+ , and He^+ , we simulate the RC dynamics by solving the bounce-averaged kinetic equation for the phase space distribution function (PSDF), $F(r_0, \varphi, E, \mu_0, t)$. The PSDF depends on the radial distance in the magnetic equatorial plane r_0 , geomagnetic east longitude φ , kinetic energy E , cosine of the equatorial pitch angle μ_0 , and time t [see, e. g., *Fok et al.*, 1993; *Jordanova et al.*, 1996]. We use the bounce-averaged kinetic equation for the He^+ -mode of EMIC waves to describe the wave power spectral density. This equation was originally derived by *Khazanov et al.* [2006], and explicitly includes the EMIC wave propagation, refraction and reflection in a multi-ion magnetospheric plasma. Following to *Khazanov et al.* [2006], we ignore the slow azimuthal and radial drifts of the waves during propagation, and use the reduced wave kinetic equation. So the resulting system of governing equations take the form:

$$\begin{aligned} \frac{\partial F}{\partial t} + \frac{1}{r_0^2} \frac{\partial}{\partial r_0} \left(r_0^2 \left\langle \frac{dr_0}{dt} \right\rangle F \right) + \frac{\partial}{\partial \varphi} \left(\left\langle \frac{d\varphi}{dt} \right\rangle F \right) + \frac{1}{\sqrt{E}} \frac{\partial}{\partial E} \left(\sqrt{E} \left\langle \frac{dE}{dt} \right\rangle F \right) \\ + \frac{1}{\mu_0 h(\mu_0)} \frac{\partial}{\partial \mu_0} \left(\mu_0 h(\mu_0) \left\langle \frac{d\mu_0}{dt} \right\rangle F \right) = \left\langle \left(\frac{\delta F}{\delta t} \right)_{loss} \right\rangle, \end{aligned} \quad (1)$$

$$\frac{\partial B_w^2(r_0, \varphi, t, \omega, \theta_0)}{\partial t} + \langle \dot{\theta}_0 \rangle \cdot \frac{\partial B_w^2}{\partial \theta_0} = 2 \langle \gamma(r_0, \varphi, t, \omega, \theta_0) \rangle \cdot B_w^2. \quad (2)$$

166 In the left-hand side of equation (1), all the bounce-averaged drift velocities are denoted
 167 as $\langle \dots \rangle$, and may be found in previous studies [*Jordanova et al.*, 1994; *Khazanov et al.*,
 168 2003]. In equation (2), ω and θ_0 are the wave frequency and equatorial wave normal
 169 angle, respectively, $\langle \dot{\theta}_0 \rangle$ is the bounce-averaged drift velocity of the equatorial wave

170 normal angle, B_w is the EMIC wave magnetic field, and $\langle \gamma \rangle$ is a result of averaging
 171 of the local growth/damping rates, which includes both the wave energy source due
 172 to interaction with RC ions and the energy sink due to absorption by thermal and
 173 hot plasmas, along the ray phase trajectory over the wave bounce period. Note that
 174 equation (2) is accompanied by a system of the ray tracing equations which are not
 175 written here (for details see *Khazanov et al.* [2006] and references therein).

176 The term in the right-hand side of equation (1) includes losses from charge
 177 exchange, Coulomb collisions, ion-wave scattering, and precipitation at low altitudes
 178 [*Jordanova et al.*, 1996, 1997; *Khazanov et al.*, 2002, 2003]. Loss through the dayside
 179 magnetopause is taken into account allowing a free outflow of the RC ions from a
 180 simulation domain. The bounce-averaged pitch angle diffusion term in the right-hand
 181 side of equation (1) is a functional of the EMIC wave power spectral density, B_w^2 , i. e.
 182 the diffusion coefficient has the form $\langle D_{\mu_0, \mu_0} \rangle = \langle D_{\mu_0, \mu_0} (B_w^2(\cdot)) \rangle$. On the other hand,
 183 $\langle \gamma \rangle$ in equation (2) is a functional of the phase space distribution function, F , i. e.
 184 $\langle \gamma \rangle = \langle \gamma (F(\cdot)) \rangle$. So equations (1) and (2) self-consistently describes the interacting
 185 RC and EMIC waves in a quasilinear approximation. It should be emphasized that in
 186 order to describe the wave-particle interaction in equation (1) we have to know the
 187 off-equatorial power spectral density distribution for EMIC waves, and this distribution
 188 can then be mapped from the magnetic equator using solutions of the ray tracing
 189 equations.

190 The geomagnetic field in our simulation is taken to be a dipole field. The electric
 191 field is expressed as the shielded (exponent 2) Volland-Stern convection field [*Volland,*

192 1973; *Stern*, 1975] which is Kp -dependent, with a corotation field [see, e. g., *Lyons and*
 193 *Williams*, 1984]. The equatorial thermal electron density distribution is calculated with
 194 the time-dependent model of *Rasmussen et al.* [1993]. For modeling the RC-EMIC
 195 wave interaction and wave propagation we also need to know the density distribution
 196 in the meridional plane. In the present study we employ an analytical density model
 197 which includes the product of three terms; (1) diffusive equilibrium model term
 198 [*Angerami and Thomas*, 1964], (2) lower ionosphere term, and (3) plasmopause and
 199 outer magnetosphere term. This analytical model is adjusted to the *Rasmussen* model
 200 at the equator. So the resulting plasmaspheric density model provides a 3D spatial
 201 distribution for electrons, and an ion content assumed to be 77% for H^+ , 20% for He^+ ,
 202 and 3% for O^+ . Geocoronal neutral hydrogen number density, needed to calculate
 203 loss due to charge exchange, is obtained from the spherically symmetric model of
 204 *Chamberlain* [1963] with its parameters given by *Rairden et al.* [1986].

205 In order to study *Dst* variation during the May 1998 storm period, and to calculate
 206 the energy content for the major RC ion species, H^+ , O^+ , He^+ , *Farrugia et al.* [2003]
 207 used the RC kinetic model of *Jordanova et al.* [1998a]. They found that during this
 208 storm the energy density of H^+ is greater than twice that of O^+ at all MLTs, and
 209 the contribution of He^+ to the RC energy content is negligible. This implies that
 210 RC O^+ content do not exceed 30% during the main phase of this storm. Note that
 211 above estimation was obtained from a simulation without oxygen band waves. On the
 212 other hand, *Bräysy et al.* [1998] observed very asymmetric O^+ RC during the main
 213 phase of the April 2–8, 1993 storm, which suggests that the RC oxygen ion loss rate is

214 considerably faster than the drift speed. This result is difficult to explain in terms of
 215 charge exchange and Coulomb scattering, and suggests that the production of EMIC
 216 waves contributes significantly to RC O^+ decay during the main and early recovery
 217 phases. In other words, due to generation of the O^+ -mode EMIC waves, most RC O^+
 218 precipitates before reaching the dusk MLT sector [Bräysy *et al.*, 1998]. Therefore, to
 219 estimate the RC O^+ content correctly, the O^+ -mode should be included in simulation,
 220 and it is likely that *Farrugia et al.* [2003] overestimated the RC O^+ content during
 221 May 1998. Anyhow, the calculations of *Thorne and Horne* [1997] clearly confirm that
 222 the above RC O^+ percentage cannot significantly suppress He^+ -mode amplification,
 223 and only slightly influences the resulting wave growth. It is for this reason we chose to
 224 initially exclude RC O^+ in our particular simulation of May 2–7, 1998, and to assume
 225 that the RC is entirely made up of energetic protons.

226 The night-side boundary condition is imposed at the geostationary distance in
 227 our model, and we use the flux measurements during the modeled event obtained from
 228 the Magnetospheric Plasma Analyzer and the Synchronous Orbit Particle Analyzer
 229 instruments on the geosynchronous LANL satellites. Then, according to *Young et al.*
 230 [1982], we divide the total flux measured at geostationary orbit between the RC H^+ ,
 231 O^+ , and He^+ depending on geomagnetic and solar activity as measured by Kp and $F_{10.7}$
 232 indices. Only the H^+ fluxes were used as a boundary condition in the simulation.

233 To obtain the self-consistent initial conditions for equations (1) and (2), the
 234 simulation was started at 0000 UT on 1 May, 1998 using a background noise level for
 235 the He^+ -mode of EMIC waves [e. g., *Akhiezer et al.*, 1975b], the statistically derived

236 quiet time RC proton energy distribution of *Sheldon and Hamilton* [1993], and the
237 initial pitch angle characteristics of *Garcia and Spjeldvik* [1985]. The initial the RC
238 and EMIC wave distributions are derived independently, and of course, have nothing
239 to do with a particular state of the magnetosphere during a simulated event. Only
240 the boundary conditions provided by the LANL satellites can be considered as data
241 reflecting a particular geomagnetic situation (and, to a certain extent, the employed
242 plasmasphere and electric field models driven by Kp). Therefore, before simulation of
243 a particular geomagnetic event can be possible, we first seek an initial state for the
244 RC and EMIC waves that is self-consistent and reflects the particular geomagnetic
245 situation. In our case, this was done by running the model code for 24 hours. In about
246 20 hours of evolution, the wave magnetic energy distribution reaches a quasistationary
247 state indicating that the RC-EMIC wave system achieves a quasi-self-consistent state.
248 (Note that 20 hours has nothing to do with the typical time for wave amplification and
249 instead reflects the minimum time needed to adjust RC and waves to each other and
250 to the real prehistory of a storm.) So the self-consistent modeling of the May 1998
251 storm period is started at 0000 UT on 2 May (24 hours after 1 May 0000 UT) using
252 solutions of equations (1) and (2) at 2400 UT on 1 May as the initial conditions for
253 further simulation.

254 3. Distribution of Plasma Density and Energy Structure of RC

255 PSDFs

256 3.1. Spatial Patterns of Plasma Density During the May 1998 Storm

257 From the results of our simulation we select seven snapshots which represent the
 258 intervals of the most enhanced plasma sheet H^+ injection into the RC region. The
 259 selected equatorial plasma density distributions are presented in Figure 1. The first row
 260 in this Figure shows the electron plasma density distribution from the *Rasmussen et al.*
 261 [1993] model, and the second row provides a sum of the corresponding plasma density
 262 from the first row and the RC H^+ density. Note that starting from high L-shell, the RC
 263 ions dominate the thermal plasma excepting a plasmaspheric drainage plume, and below
 264 we shell concentrate only on cases of pronounced density enhancement during plasma
 265 sheet ion injections. The first plasma sheet ion injection appears about 32 hours after 1
 266 May, 0000 UT (not shown), which affects the density distribution for about 16 hours,
 267 while the RC ions only slightly modify the plasma density distribution after 48 hours
 268 (not shown). During this interval, the RC H^+ density dominates the thermal plasma
 269 in the dusk-midnight MLT sector (see hours 33 and 34 in Figure 1). The second ion
 270 injection starts about 56 hours (not shown). The snapshots at hour 60 show the most
 271 distinct pattern of the cold and total plasma density during this injection event when
 272 the RC H^+ dominates the thermal plasma density in the nightside through the entire
 273 dusk-dawn MLT sector. Again, there are only minor differences between the density
 274 snapshots at 68 hours (not shown). The third plasma sheet ion injection shown in

Figure 1

275 Figure 1 starts at about 76 hours and impacts the plasma density distribution through
276 hour 90 (not shown). This injection is most intense comparing to previous ones, and
277 the RC H^+ dominance is observed in the greatest L-shell and MLT extents encircling
278 a great part of the globe during the third injection. The results of our simulation are
279 in qualitative agreement with the RC density distribution obtained by *Zaharia et al.*
280 [2006] during the moderate geomagnetic storm of 21–23 April 2001.

281 We presented only the RC H^+ density distribution above, and did not say
282 anything about the distribution of the electron density. It is obvious that in all “slow”
283 magnetospheric processes the quasi-neutrality condition should hold. This implies
284 that electrons have the same density distribution as the ions. Quasi-neutrality can
285 be sustained by both the energetic plasma sheet electrons injected along with ions,
286 and/or the cold ionospheric electrons due to field-aligned currents. The resulting
287 electron temperature strongly affects the Coulomb energy degradation of the RC ions,
288 the resonant Landau damping of EMIC waves, and barely influences the EMIC wave
289 dispersive properties (see, e. g., *Khazanov et al.* [2007], *Akhiezer et al.* [1975a]).
290 *Khazanov et al.* [2007] demonstrated that both the EMIC wave Landau damping and
291 collisional RC energy dissipation are maximized for an electron temperature about
292 1 eV. This is the temperature adopted in our RC-EMIC wave model for thermal plasma
293 [*Khazanov et al.*, 2003]. Therefore, if we do not track the electron dynamics and keep
294 $T_e = 1$ eV for the entire simulation domain, we can potentially underestimate the EMIC
295 wave energy, especially at high L-shells during the main and recovery storm phases when
296 RC ions dominate the thermal plasma. Below we assume that plasma is quasi-neutral

297 and that the electron temperature is 1 eV throughout the entire simulation domain
 298 during the May 1998 event.

299 3.2. Fine Energy Structure of RC PSDFs

300 The new RC ions, injected from the plasma sheet in the night MLT sector, cause
 301 impressive plasma density enhancement for high L-shells during the main and recovery
 302 storm phases. This feature is clearly observed in our simulation, but in Figure 1 we
 303 presented only the RC H^+ density distribution, and did not analyze the fine PSDF
 304 energy structure. To consider the energy distributions of the RC H^+ , we selected four
 305 representative cases among the snapshots in Figure 1. The corresponding PSDFs are
 306 shown in Figure 2. All the PSDFs are taken in the equatorial plane, and integrated over
 307 the entire solid angle, while the effective RC proton temperature parallel to geomagnetic
 308 field line, T_{\parallel} , is calculated for the entire energy range (100 eV – 430 keV). In order to
 309 more clearly demonstrate change in the PSDF slope, we use a linear energy scale in a
 310 low energy domain of the distribution, whereas the high energy part is depicted with
 311 a logarithmic energy scale. As follows from the left-hand side of Figure 2, there is a
 312 transition region in all the PSDFs which separates relatively warm ions from the more
 313 hot and tenuous component. (The transition from a steep profile to more horizontal
 314 profile corresponds to the transition from a small to a higher effective ion temperature.)
 315 So we observe at least two ion populations which constitute the plotted RC ion PSDFs;
 316 (1) the dense and relatively cold low energy RC component, and (2) the rare and
 317 hotter high energy RC component. The boundary between these two ion components

Figure 2

318 is located at slightly different energy depending on each case, which from Figure 2, is
 319 about 1 – 1.5 keV. Note that PSDFs at hours 80 and 82 include, respectively, four and
 320 three ion populations with different effective temperatures; the PSDF taken at hour 80
 321 changes slope at energies near 1, 10, and 130 keV, whereas the PSDF at hour 82 changes
 322 slope near 0.5 and 20 keV. So the results in Figure 2 clearly demonstrate that plasma
 323 density modification due to the plasma sheet H^+ injection into the RC region is mostly
 324 caused by low energy ions with energy $\lesssim 1$ keV.

325 4. Effect of Plasma Density on EMIC Wave Growth

326 The effective proton temperatures transverse to T_{\perp} , and along T_{\parallel} , the geomagnetic
 327 field line, comply with the inequality $T_{\perp} > T_{\parallel}$ in many space plasma regimes. If the ion
 328 temperature anisotropy, $A = T_{\perp}/T_{\parallel} - 1$, exceeds some positive threshold, EMIC waves
 329 can be unstable [*Kennel and Petschek*, 1966; *Cornwall et al.*, 1970]. The growth rate
 330 for these waves critically depends on the characteristic energy for cyclotron interaction,
 331 which, as defined by *Kennel and Petschek* [1966], is just the local geomagnetic field
 332 energy per particle, having the form $E_c = B^2/(8\pi n_e)$. So, according to *Kennel and*
 333 *Petschek* [1966], the local growth rate for EMIC waves should be particularly sensitive
 334 to the local plasma density. Assuming that the RC is entirely made up of energetic H^+ ,
 335 Figure 3 plots the dependence on plasma density of the local equatorial growth/damping
 336 rate for the He^+ -mode EMIC waves. Note that the calculated growth/damping rates
 337 in Figure 3 are due to the RC-wave interaction only, and the wave absorption due to
 338 thermal plasma is omitted (but, of course, this effect is included in global simulation).

Figure 3

339 All the results in Figure 3 are obtained for the wave frequency $\nu = 0.475$ Hz, and case
 340 (a) is just taken from our global model without any modification at location $L=5.25$,
 341 $MLT=15$ at 48 hours ($n_e = n_0 = 68.3 \text{ cm}^{-3}$, and $B = 215.3 \text{ nT}$). In order to produce
 342 the results (b), (c), and (d), we need only re-normalize the local plasma density as
 343 $n_e = 1.2 \times n_0$, $n_e = 1.5 \times n_0$, and $n_e = 2.0 \times n_0$, respectively. As follows from Figure 3,
 344 transitioning from case (a) to case (b) increases the peak growth rate by a factor 1.4,
 345 extends the region of growth, and makes the wave damping negligible. Further increase
 346 of the number density eliminates the region of wave damping. According to [Kennel and
 347 *Petschek*, 1966], the growth rate dependence on plasma density is $\gamma \sim \exp(-1/n_e)/\sqrt{n_e}$.
 348 So, although the characteristic energy decreases with increasing plasma density, the
 349 growth rate can both increase or decrease depending on the wave normal angle (see
 350 Figure 3). For a particular wave normal angle, it depends on whether we move to the
 351 growth rate maximum with density increase or whether we move from the maximum.

352 5. Effects of RC Temperature on EMIC Wave He^+ -Mode

Although the results presented in subsection 3.2 clearly demonstrate that the
 observed plasma density enhancement is caused by a low energy ($\lesssim 1 \text{ keV}$) population
 of the RC, this does not allow us to evaluate the effects of the RC ion temperature on
 the EMIC wave dispersive properties. In order to characterize the temperature effects
 in the EMIC wave dispersion relation, we use the following parameters [see, e. g., *Stix*,

1992; Akhiezer et al., 1975a]

$$\lambda_i = \left(\frac{k_{\perp} v_{\perp,i}}{\sqrt{2}\Omega_i} \right)^2, \quad \zeta_i = \left(\frac{\omega \pm \Omega_i}{k_{\parallel} v_{\parallel,i}} \right)^2, \quad i = e, H^+, He^+, O^+, \quad (3)$$

353 where Ω_i is the particle gyrofrequency, and k_{\perp} ($v_{\perp,i} = \sqrt{2T_{\perp,i}/m_i}$) and k_{\parallel} ($v_{\parallel,i} =$
354 $\sqrt{2T_{\parallel,i}/m_i}$) are the components of the wave normal vector (thermal velocity) transverse
355 to and along geomagnetic field lines, respectively; λ_i is the squared ratio of Larmor
356 radius to transverse wave length; and ζ_i is the squared ratio of longitudinal wave length
357 to a typical particle displacement along the field line during a wave period. The finite
358 Larmor radius effects are negligible if $\lambda_i \ll 1$. On the other hand, the plasma particles
359 become unmagnetized if $\lambda_i \gg 1$, and as a consequence the external magnetic field
360 disappears in the wave dispersion relation. So the Larmor radius effects are most
361 important for an intermediate case when the wave and particle parameters give $\lambda_i \sim 1$.
362 The magnitude of ζ_i not only characterizes the importance of “longitudinal” thermal
363 effects, but also determines the effectiveness of the resonant wave damping/growth. For
364 instance, the number of resonating particles is small if $\zeta_i \gg 1$, and as a result, plasma
365 waves can exist for a long time without substantial damping. So the role of thermal
366 effects in the wave dispersion relation depends on the magnitude of both ζ_i and λ_i . For
367 example, if these parameters comply with the inequalities $\lambda_i \ll 1$ and $\zeta_i \gg 1$, in many
368 cases (but not always!) the leading term in a real part of dispersion relation still comes
369 from a cold plasma approximation (limit $\lambda_i = 0$ and $\zeta_i \rightarrow \infty$, e. g., *Stix* [1992]). So
370 depending on the magnitudes of ζ_i and λ_i , the thermal terms may be a minor correction
371 only, or they can dominate the “cold plasma limit” term.

372 Until now, we discussed only the RC H^+ . Although the RC H^+ dominate both O^+
 373 and He^+ during the May 1998 storm [Farrugia *et al.*, 2003], and we do not simulate the
 374 RC O^+ and He^+ in the present study, the heavy ions participate in the RC dynamics
 375 and can influence the magnetospheric heavy ion content, especially during the main and
 376 early recovery storm phases. Despite the importance of the hot heavy ions for the EMIC
 377 wave characteristics (see, e. g., Kozyra *et al.* [1984]), in all previous studies we assumed
 378 that the total ion composition is dominated by the ion composition of the thermal
 379 plasma and did not take into account the RC ions in the real part of the wave dispersion
 380 relation [Khazanov *et al.*, 2002, 2003, 2006, 2007], including the RC ions in the imaginary
 381 part only. In all those papers, when we described the EMIC wave dispersive properties
 382 we used the electron density distribution from the time-dependent Rasmussen *et al.*
 383 [1993] model, and the ion content was assumed to be 77% for H^+ , 20% for He^+ , and
 384 3% for O^+ . (Although the assumed ion content is in the range of 10 – 30% for He^+
 385 and 1 – 5% for O^+ following observations by Young *et al.* [1983, 1977] and Horwitz *et*
 386 *al.* [1981], it only approximately describes the real ion percentage and, of course, does
 387 not reflect its variability, especially during the magnetically active periods.) Now we are
 388 going to take into account the RC ions in the real part of the EMIC wave dispersion
 389 relation which can strongly modify the heavy ion percentage. In spite of this, for the
 390 purpose of comparison with previous results, we keep the earlier adopted ion percentage
 391 (77% for H^+ , 20% for He^+ , and 3% for O^+) throughout the entire simulation domain
 392 even if this percentage is mainly determined by the suprathermal/hot ion composition.

It follows from equation (3), assuming that all the RC ions (H^+ , He^+ , O^+) have

nearly the same temperature, that parameters λ_i relate to each other as masses of the corresponding RC ions. Then, considering the most dense suprathermal spots in Figure 1, we find that for the He^+ -mode the following inequality

$$\lambda_{H^+} < \lambda_{He^+} < \lambda_{O^+} \ll 1 \ll \zeta_{He^+} \lesssim \zeta_{O^+} \ll \zeta_{H^+} \quad (4)$$

holds. Note that in order to obtain inequalities (4), we used $v_{\perp,i}$ and $v_{\parallel,i}$ calculated for the entire energy range; parameters λ_i and ζ_i could be even closer to the cold plasma limit if all the effective temperatures are calculated for a low energy RC component only (see subsection 3.2), which gives the greatest contribution to the plasma density enhancement observed in night side during the main and recovery storm phases. In the limit (4), the structure of thermal terms in the EMIC wave dispersion equation can be found, e. g., in [Stix, 1992; Akhiezer et al., 1975a] where the finite Larmor radius effects may be omitted. The greatest thermal term (Λ_{\parallel}) in the dispersion equation for the EMIC wave He^+ -mode comes from the RC H^+ during the May 1998 storm with the following ranking

$$\Lambda_{\parallel}(H^+) \gg \Lambda_{\parallel}(O^+) \sim \Lambda_{\parallel}(He^+). \quad (5)$$

393 So only term $\Lambda_{\parallel}(H^+)$ can potentially compete with the “cold plasma limit” term in
 394 the He^+ -mode dispersion equation. Considering the most dense suprathermal spots
 395 in Figure 1, we find that $\Lambda_{\parallel}(H^+)$, as a rule, can be neglected in comparison with the
 396 “cold” term in the He^+ -mode dispersion relation.

397 6. Results and Discussions

398 Summarizing all the assumptions and conclusions we did in sections 3 and 5:
 399 (1) Plasma is quasi-neutral (see subsection 3.1); (2) the electron temperature is
 400 1 eV through the entire simulation domain (subsection 3.1); (3) the plasma density
 401 enhancement observed in Figure 1 is caused by a low energy ($\lesssim 1$ keV) population of
 402 the RC ions (subsection 3.2), while the RC H^+ ions dominate both the RC O^+ and
 403 He^+ during May 1998; (4) the ion percentage is 77% for H^+ , 20% for He^+ , and 3%
 404 for O^+ through the entire simulation domain (section 5); and (5) the thermal effects of
 405 electrons and the RC ions may be neglected in the real part of the He^+ -mode dispersion
 406 relation (see subsections 3.1 and section 5).

407 6.1. Global Distribution of He^+ -Mode

The equatorial (MLT, L-shell) distributions of the squared wave magnetic field,

$$B_w^2(r_0, \varphi, t) = \int_{\omega_{min}}^{\omega_{max}} d\omega \int_0^\pi d\theta_0 B_w^2(r_0, \varphi, t, \omega, \theta_0), \quad (6)$$

408 are shown in Figure 4 for the He^+ -mode of EMIC waves. These simulation results
 409 are based on the system of governing equations (1) and (2) along with the ray tracing
 410 equations. The results in the first row are obtained when the RC ions are only treated
 411 as a source of free energy to generate EMIC waves, and omitted in the real part of the
 412 wave dispersion relation. The second row shows the case when the RC ions are taken
 413 into account in both the real and imaginary parts of the wave dispersion relation. There
 414 is an essential difference between the EMIC wave energy distributions in the first and

Figure 4

415 second rows. Modification of the EMIC wave dispersive properties due to RC ions leads
416 to a relatively minor spatial redistribution of the “old” wave active zones presented in
417 the first row, and mainly alters the wave intensities. The qualitative difference between
418 the first and second rows appears during the recovery phase in the postmidnight–dawn
419 MLT sector for $L > 4.75$ (hours 82 and 84). In these regions, “new” EMIC waves are
420 generated due to modification of the wave dispersion by RC, and we do not observe any
421 wave activity in corresponding snapshots in the first row. The B–field distributions are
422 organized by the locations of sharp gradient in the total density of thermal plasma and
423 RC as expected from previous studies [*Horne and Thorne, 1993; Khazanov et al., 2006*].
424 (The sharp density drop counteracts the refraction caused by the magnetic field gradient
425 and curvature. As a result, net refraction is suppressed, and the He^+ –mode grows
426 preferentially at these locations.) At the same time, we note that a radial extension of
427 wave zones in the second row is slightly greater than that in the first row.

428 Let us now discuss the new feature caused by the modified EMIC wave dispersion
429 and clearly observed in Figure 4. Recently, *Engebretson et al. [2007]* presented
430 measurements of EMIC waves in the Pc 1–2 frequency range and the associated ion
431 distributions obtained Cluster. During the October and November 2003 magnetic
432 storms, the most intense waves were observed on 22 November near the end of a rapid
433 recovery phase from 0825 to 0850 UT; located near dawn for $L=4.4$ – 4.6 and at an
434 average MLAT $\approx 18^\circ$. The waves were primarily transverse, propagated away from
435 the equator, and predominantly left–hand polarized. Compared to the local proton
436 gyrofrequency, these waves had a normalized frequency of $X=0.34$, somewhat higher

437 than the local He^+ gyrofrequency ($X=0.25$). The free energy to generate those waves
 438 was associated with anisotropic RC H^+ of energies greater than 10 keV. Note that the
 439 upper energy range of increased energy fluxes may well extend beyond the 40 keV limit
 440 of the Cluster CIS instrument. Although the temperature anisotropy of these energetic
 441 (> 10 keV) protons was high during the entire 22 November pass, EMIC waves were
 442 observed only in conjunction with intensification of the ion fluxes below 1 keV by over
 443 an order of magnitude. This suggests that the suprathermal plasma plays an important
 444 role in the destabilization of the more energetic RC and/or plasma sheet ions, and the
 445 high energy anisotropic RC and/or plasma sheet proton distributions appeared to be
 446 a necessary but not sufficient condition for the occurrence of EMIC waves. Similarly,
 447 studying Pc 1-2 events on the dayside outer magnetosphere, *Engebretson et al.* [2002]
 448 and *Arnoldy et al.* [2005] found that greatly increased fluxes of low energy protons are
 449 crucial for the destabilization of the high energy anisotropic RC protons.

450 The satellite observations by *Engebretson et al.* [2007] support our theoretical
 451 results presented in Figure 4. Indeed, in the second row we see intense EMIC waves (up
 452 to a few nT^2) in the postmidnight-dawn sector (for $L > 4.75$) during the recovery phase
 453 from 82 to 84 hours. This wave activity is not observed if the RC ions are not included
 454 in the real part of the wave dispersion relation (compare the first and second rows in
 455 Figure 4). At the same time, we note that *Engebretson et al.* [2007] observed waves with
 456 a normalized frequency $X=0.34$, whereas we consider the He^+ -mode of EMIC waves
 457 with $X < 0.25$. (The most intense burst of Pc 1 waves studied by *Arnoldy et al.* [2005]
 458 was measured by the Polar satellite with a local normalized frequency of $X=0.2$, so the

459 waves were also He^+ -mode.) For the purpose of comparison with previous results, in
 460 the present study we kept the ion percentage the same as in our earlier studies, namely,
 461 77% for H^+ , 20% for He^+ , and 3% for O^+ . Then the most effective generation takes
 462 place for the He^+ -mode in the frequency range $\Omega_{O^+} < \omega < \Omega_{He^+}$ [see, e. g., *Kozyra et*
 463 *al.*, 1984; *Horne and Thorne*, 1993; *Khazanov et al.*, 2003]. (Note that only waves in
 464 the left-hand polarized part of the dispersive surface can grow, and the corresponding
 465 wave frequencies should be in the range between the cross-over frequency and Ω_{He^+} .)
 466 This heavy ion content, however, differs strongly from the ion percentage reported by
 467 *Engebretson et al.* [2007]. For example, they observed 81% of H^+ , 3% of He^+ , and 16%
 468 of O^+ on November 22, 2003 at 0740 UT, qualitatively different from the percentage
 469 we used in the simulation. Such a great amount of RC O^+ , in combination with small
 470 amounts of He^+ , should suppress the He^+ -mode, and conversely favor the H^+ -mode.
 471 Self-consistent modeling of the H^+ -mode is beyond the scope of the current study, and
 472 should be done separately. (Strictly speaking, EMIC waves are very sensitive to the
 473 the heavy ions, so wave simulation requires more realistic dynamic models of the global
 474 distribution for each ion species which, unfortunately, are currently not available.) At
 475 present, we believe that the crucial role of low energy RC and/or plasma sheet protons
 476 in the destabilization of the high energy anisotropic RC protons is well established both
 477 experimentally and theoretically. We also think that this feature depends on the wave
 478 mode only quantitatively, and the qualitative effect itself does not depend on the wave
 479 mode.

480 6.2. Wave-Induced RC Precipitation

One of the most pronounced consequences of the RC-EMIC wave interaction is the scattering of RC ions into the loss cone. This process is one of the processes that lead to decay of RC [see, e. g., *Cornwall et al.*, 1970], especially during the main and early recovery phases of storms when decay time of about one hour or less is possible [*Gonzalez et al.*, 1989]. The EMIC wave-induced RC precipitation was studied widely both experimentally and theoretically [e. g., *Erlandson and Ukhorskiy*, 2001; *Yahnina et al.*, 2003; *Walt and Voss*, 2001, 2004; *Jordanova et al.*, 2001]. Although the effect of EMIC waves on RC ion precipitation during the May 1998 storm was discussed previously [e. g., *Khazanov et al.*, 2002, 2007], we present a few precipitating patterns that demonstrate the new features caused by modification of the EMIC wave dispersion relation. The RC precipitating flux is calculated as

$$J_{lc} = \frac{1}{\Omega_{lc}} \int_{E_1}^{E_2} dE \int_{\mu_{lc}}^1 d\mu_0 j, \quad \Omega_{lc} = \int_{\mu_{lc}}^1 d\mu_0, \quad (7)$$

481 where μ_{lc} is the cosine of the equatorial pitch angle at the boundary of loss cone, and
 482 j is the equatorial ion differential flux. In Figure 5 we show selected snapshots of the
 483 precipitating fluxes integrated over the energy range 1 – 50 keV. As before, the first
 484 row shows the results without the RC ions in the real part of the EMIC wave dispersion
 485 relation, while the second row shows precipitation when the RC ions are taken into
 486 account in both the real and imaginary parts of the wave dispersion relation. There are
 487 many differences between the first and second rows. The most intense ion precipitation
 488 is due to “new” wave activity, and located in the night MLT sector. The strongest

Figure 5

489 fluxes of about $8 \cdot 10^6 \text{ (cm}^2 \cdot \text{s} \cdot \text{sr)}^{-1}$ are observed near $L=5.75$, $\text{MLT}=2$ during the early
 490 recovery phase of the storm (see hour 82 in Figure 5). This precipitation is two times
 491 greater than a greatest flux from a previous study of the May 1998 storm by *Khazanov*
 492 *et al.* [2007]. The very interesting result can be derived by comparing Figure 5 with
 493 Figure 4; the wave-induced night side precipitation is more intense than the day side
 494 fluxes, even if there are less intense waves (compare locations $L=4.5$, $\text{MLT}=16$, and
 495 $L=5.75$, $\text{MLT}=2$ in the 82 hour snapshots). The major reason for this feature is a
 496 magnetospheric convection field which acts oppositely in day and in night sides moving
 497 RC ions into the loss cone on the nightside, and driving them out of the loss cone
 498 on the dayside. So the magnetospheric convection and the wave scattering reinforce
 499 each other on the nightside, but subtract on the dayside. Of course, we have to recall
 500 that characteristics of the wave normal angle distribution can strongly impact the
 501 effectiveness of RC ion scattering [*Khazanov et al.*, 2007].

502 7. Conclusions

503 In this paper we have further developed a self-consistent model of RC ions and
 504 propagating EMIC waves by *Khazanov et al.* [2006]. We have taken into account RC
 505 ions in the real part of dispersion relation for the He^+ -mode of EMIC waves. This is a
 506 new feature of the present model and generalizes the limiting assumption that the total
 507 plasma density was dominated by the thermal plasma made by all previous RC-EMIC
 508 wave models, so that the RC ions were not taken into account in the real part of the
 509 wave dispersion relation [*Kozyra et al.*, 1997; *Jordanova et al.*, 1998b, 2001; *Khazanov*

510 *et al.*, 2003, 2006] but only in the imaginary part, i. e., in the EMIC wave growth rate.
 511 This assumption is not always valid, especially for high L-shells during the main and
 512 recovery storm phase when the newly injected RC ions dominate the thermal plasma
 513 (see results of our simulation in Figure 1). Recent satellite observations during the
 514 November 2003 magnetic storm by *Engebretson et al.* [2007] showed that although
 515 the temperature anisotropy of energetic (> 10 keV) RC protons was high during the
 516 entire 22 November 2003 perigee pass, EMIC waves were observed only in conjunction
 517 with intensification of the ion fluxes below 1 keV by over an order of magnitude. This
 518 suggests that the suprathermal plasma ($\lesssim 1$ keV) plays an important role in the
 519 destabilization of the more energetic RC and/or plasma sheet ions such that high energy
 520 anisotropic RC and/or plasma sheet proton distributions appeared to be a necessary
 521 but not sufficient condition for occurrence of EMIC waves.

522 To demonstrate the role of RC ions in the real part of EMIC wave dispersion
 523 relation, we have simulated the May 1998 storm, and have presented and discussed
 524 the global distributions of the total plasma density, the energy of the He^+ -mode, and
 525 the wave-induced RC precipitation. The main conclusions of our simulation can be
 526 summarized as follows.

527 1. The new RC ions, injected from the plasma sheet in the night MLT sector, causes
 528 plasma density enhancements for high L-shells during the main and recovery storm
 529 phases. This feature is clearly observed in our simulation (see Figure 1), and the plasma
 530 density enhancement is mostly caused by the suprathermal H^+ ($\lesssim 1$ keV).

531 2. During the recovery phase, modification of the wave dispersion relation by RC

532 ions leads to a dramatic change in the wave patterns in the nightside MLT sector for
533 $L > 4.75$.

534 3. The Cluster observations of EMIC waves and associated ion distributions during
535 the November 2003 magnetic storm [Engebretson *et al.*, 2007] support our theoretical
536 results presented in Figure 4. In the second row of Figure 4 we see intense EMIC waves
537 (up to a few nT^2) in the postmidnight–dawn sector during the recovery storm phase
538 from 82 to 84 hours. This wave activity is not observed if the RC ions are not included
539 in the real part of the wave dispersion relation (compare the first and second rows in
540 Figure 4).

541 4. The most intense wave-induced RC precipitation is due to modification of the
542 wave dispersion relation, located in the night MLT sector. The strongest precipitating
543 fluxes of about $8 \cdot 10^6 \text{ (cm}^2 \cdot \text{s} \cdot \text{sr)}^{-1}$ are observed near $L=5.75$, $\text{MLT}=2$ during the early
544 recovery phase of the storm (see hour 82 in Figure 5). The wave-induced nightside
545 precipitation is more intense than the dayside fluxes, even if there are less intense
546 waves (compare the results at $L=4.5$, $\text{MLT}=16$, and $L=5.75$, $\text{MLT}=2$ in the 82 hour
547 snapshots).

548 **Acknowledgments.** This research was performed while K. Gamayunov held a NASA
549 Postdoctoral Program appointment at NASA/MSFC. Funding in support of this study was
550 provided by NASA grant UPN 370–16–10.

551 **References**

- 552 Akhiezer, A. I., I. A. Akhiezer, R. V. Polovin, A. G. Sitenko, and K. N. Stepanov
553 (1975a), *Plasma Electrodynamics*, vol. 1, Pergamon, Tarrytown, N. Y.
- 554 Akhiezer, A. I., I. A. Akhiezer, R. V. Polovin, A. G. Sitenko, and K. N. Stepanov
555 (1975b), *Plasma Electrodynamics*, vol. 2, Pergamon, Tarrytown, N. Y.
- 556 Albert, J. M. (2003), Evaluation of quasi-linear diffusion coefficients for EMIC waves in a
557 multispecies plasma, *J. Geophys. Res.*, *108*, A6, 1249, doi:10.1029/2002JA009792.
- 558 Anderson, B. J., R. E. Erlandson, and L. J. Zanetti (1992a), A statistical study of
559 Pc 1–2 magnetic pulsations in the equatorial magnetosphere: 1. Equatorial
560 occurrence distributions, *J. Geophys. Res.*, *97*, 3075.
- 561 Anderson, B. J., R. E. Erlandson, and L. J. Zanetti (1992b), A statistical study of Pc
562 1–2 magnetic pulsations in the equatorial magnetosphere: 2. Wave properties, *J.*
563 *Geophys. Res.*, *97*, 3089.
- 564 Anderson, B. J., and S. A. Fuselier (1994), Response of thermal ions to electromagnetic
565 ion cyclotron waves, *J. Geophys. Res.*, *99*, 19413.
- 566 Angerami, J. J., and J. O. Thomas (1964), Studies of planetary atmospheres, 1, The
567 distribution of ions and electrons in the earth's exosphere, *J. Geophys. Res.*, *69*,
568 4537.
- 569 Arnoldy, R. L., M. J. Engebretson, R. E. Denton, J. L. Posch, M. R. Lessard, N.
570 C. Maynard, D. M. Ober, C. J. Farrugia, C. T. Russell, J. D. Scudder, R. B.
571 Torbert, S.-H. Chen, and T. E. Moore (2005) Pc 1 waves and associated unstable

- 572 distributions of magnetospheric protons observed during a solar wind pressure
573 pulse, *J. Geophys. Res.*, *110*, A07229, doi:10.1029/2005JA011041.
- 574 Bezrukikh, V. V., and K. I. Gringauz (1976), The hot zone in the outer plasmasphere of
575 the Earth, *J. Atmos. Terr. Phys.*, *38*, 1085.
- 576 Bräysy, T., K. Mursula, and G. Marklund (1998), Ion cyclotron waves during a great
577 magnetic storm observed by Freja double-probe electric field instrument, *J.*
578 *Geophys. Res.*, *103*, 4145.
- 579 Chamberlain, J. W. (1963), Planetary corona and atmospheric evaporation, *Planet.*
580 *Space Sci.*, *11*, 901.
- 581 Cornwall, J. M. (1964), Cyclotron instabilities and electromagnetic emission generation
582 mechanisms, *J. Geophys. Res.*, *69*, 4515.
- 583 Cornwall, J. M. (1965), Cyclotron instabilities and electromagnetic emission in the ultra
584 low frequency and very low frequency ranges, *J. Geophys. Res.*, *70*, 61.
- 585 Cornwall, J. M., F. V. Coroniti, and R. M. Thorne (1970), Turbulent loss of ring current
586 protons, *J. Geophys. Res.*, *75*, 4699.
- 587 Cornwall, J. M., F. V. Coroniti, and R. M. Thorne (1971), Unified theory of SAR arc
588 formation at the plasmopause, *J. Geophys. Res.*, *76*, 4428.
- 589 Denton, R. E., M. K. Hudson, and I. Roth (1992), Loss-cone-driven ion cyclotron waves
590 in the magnetosphere, *J. Geophys. Res.*, *97*, 12093.
- 591 Engebretson, M. J., A. Keiling, K.-H. Fornacon, C. A. Cattell, J. R. Johnson, J. L.
592 Posch, S. R. Quick, K.-H. Glassmeier, G. K. Parks, and H. Réme (2007), Cluster
593 observations of Pc 1–2 waves and associated ion distributions during the October

- 594 and November 2003 magnetic storms, *Planet. Space Sci.*, *55*, 6, 829.
- 595 Engebretson, M. J., W. K. Peterson, J. L. Posch, M. R. Klatt, B. J. Anderson, C. T.
596 Russell, H. J. Singer, R. L. Arnoldy, H. Fukunishi (2002), Observations of two
597 types of Pc 1–2 pulsations in the outer dayside magnetosphere, *J. Geophys. Res.*,
598 *107*, A12, 1451, doi:10.1029/2001JA000198.
- 599 Engebretson, M. J., J. L. Posch, M. R. Lessard, R. L. Arnoldy, D. E. Rowland,
600 S.–H. Chen, T. E. Moore, W. K. Peterson, T. G. Onsager, J. R. Johnson,
601 and C. T. Russell (2005), Pc 1 waves and associated unstable distributions
602 of magnetospheric protons during three extended conjunctions between the
603 Polar satellite and Antarctic ground stations, *IAGA Meeting*, Toulouse, France,
604 July 25, 2005.
- 605 Erlandson, R. E., and A. J. Ukhorskiy (2001), Observations of electromagnetic ion
606 cyclotron waves during geomagnetic storms: Wave occurrence and pitch angle
607 scattering, *J. Geophys. Res.*, *106*, 3883.
- 608 Erlandson, R. E., L. J. Zanetti, T. A. Potemra, L. P. Block, and G. Holmgren (1990),
609 Viking magnetic and electric field observations of Pc 1 waves at high latitudes,
610 *J. Geophys. Res.*, *95*, 5941.
- 611 Farrugia, C. J., V. K. Jordanova, M. P. Freeman, C. C. Cochei, R. L. Arnoldy,
612 M. Engebretson, P. Stauning, G. Rostoker, M. F. Thomsen, G. D. Reeves, and
613 K. Yumoto (2003), Large-scale geomagnetic effects of May 4, 1998, *Adv. Space*
614 *Res.*, *31/4*, 1111.
- 615 Foat, J. E., R. P. Lin, D. M. Smith, F. Fenrich, R. Millan, I. Roth, K. R. Lorentzen,

- 616 M. P. McCarthy, G. K. Parks, and J. P. Treilhou (1998), First detection of a
617 terrestrial MeV X-ray burst, *Geophys. Res. Lett.*, *25*, 4109.
- 618 Fok, M.-C., J. U. Kozyra, A. F. Nagy, C. E. Rasmussen, and G. V. Khazanov (1993),
619 A decay model of equatorial ring current and the associated aeronomical
620 consequences, *J. Geophys. Res.*, *98*, 19381.
- 621 Fraser, B. J., and T. S. Nguyen (2001), Is the plasmopause a preferred source region of
622 electromagnetic ion cyclotron waves in the magnetosphere?, *J. Atmos. Sol. Terr.*
623 *Phys.*, *63*, 1225.
- 624 Fuselier, S. A., and B. J. Anderson (1996) Low-energy He^+ and H^+ distributions and
625 proton cyclotron waves in the afternoon equatorial magnetosphere, *J. Geophys.*
626 *Res.*, *101*, 13255.
- 627 Galeev, A. A. (1975), Plasma turbulence in the magnetosphere with special regard to
628 plasma heating, in *Physics of the Hot Plasma in the Magnetosphere*, edited by B.
629 Hultquist, and L. Stenflo, p. 251, Plenum Press, N. Y.-London.
- 630 Garcia, H. A., and W. N. Spjeldvik (1985), Anisotropy characteristics of geomagnetically
631 trapped ions, *J. Geophys. Res.*, *90*, 347.
- 632 Gendrin, R., M. Ashour-Abdalla, Y. Omura, and K. Quest (1984), Linear analysis of
633 ion-cyclotron interaction in a multicomponent plasma, *J. Geophys. Res.*, *89*,
634 9119.
- 635 Gomberoff, L., and R. Neira (1983), Convective growth rate of ion cyclotron waves in a
636 $H^+ - He^+$ and $H^+ - He^+ - O^+$ plasma, *J. Geophys. Res.*, *88*, 2170.
- 637 Gonzalez, W. D., B. T. Tsurutani, A. L. C. Gonzalez, E. J. Smith, F. Tang, and S.-I.

- 638 Akasofu (1989), Solar wind-magnetosphere coupling during intense magnetic
639 storms (1978–1979), *J. Geophys. Res.*, *94*, 8835.
- 640 Gorbachev, O. A., G. V. Khazanov, K. V. Gamayunov, and E. N. Krivorutsky (1992), A
641 theoretical model for the ring current interaction with the Earth's plasmasphere,
642 *Planet. Space Sci.*, *40*, 859.
- 643 Gringauz, K. I. (1983), Plasmasphere and its interaction with ring current, *Space Sci.*
644 *Rev.*, *34*, 245.
- 645 Gringauz, K. I. (1985), Structure and properties of the Earth plasmasphere, *Adv. Space*
646 *Res.*, *5*, 391.
- 647 Gurgiolo, C., B. R. Sandel, J. D. Perez, D. G. Mitchell, C. J. Pollock, and B. A. Larsen
648 (2005), Overlap of the plasmasphere and ring current: Relation to subauroral
649 ionospheric heating, *J. Geophys. Res.*, *110*, A12217, doi:10.1029/2004JA010986.
- 650 Horne, R. B., and R. M. Thorne (1993), On the preferred source location for the
651 convective amplification of ion cyclotron waves, *J. Geophys. Res.*, *98*, 9233.
- 652 Horne, R. B., and R. M. Thorne (1997), Wave heating of He^+ by electromagnetic ion
653 cyclotron waves in the magnetosphere: Heating near $H^+ - He^+$ bi-ion resonance
654 frequency, *J. Geophys. Res.*, *102*, 11457.
- 655 Horwitz, J. L., C. R. Baugher, C. R. Chappell, E. G. Shelley, D. T. Young, and R.
656 R. Anderson (1981), ISEE 1 observations of thermal plasma during periods of
657 quieting magnetic activity, *J. Geophys. Res.*, *86*, 9989.
- 658 Iyemori, T., and K. Hayashi (1989), Pc 1 micropulsations observed by Magsat in
659 ionospheric F region, *J. Geophys. Res.*, *94*, 93.

- 660 Jordanova, V. K., C. J. Farrugia, L. Janoo, J. M. Quinn, R. B. Torbert, K. W. Ogilvie,
661 R. P. Lepping, J. T. Steinberg, D. J. McComas, and R. D. Belian (1998a),
662 October 1995 magnetic cloud and accompanying storm activity: Ring current
663 evolution, *J. Geophys. Res.*, *103*, 79.
- 664 Jordanova, V. K., C. J. Farrugia, J. M. Quinn, R. M. Thorne, K. W. Ogilvie, R. P.
665 Lepping, G. Lu, A. J. Lazarus, M. F. Thomsen, and R. D. Belian (1998b), Effect
666 of wave-particle interactions on ring current evolution for January 10–11, 1997:
667 Initial results, *Geophys. Res. Lett.*, *25*, 2971.
- 668 Jordanova, V. K., C. J. Farrugia, R. M. Thorne, G. V. Khazanov, G. D. Reeves, and
669 M. F. Thomsen, Modeling ring current proton precipitation by EMIC waves
670 during the May 14–16, 1997, storm, *J. Geophys. Res.*, *106*, 7, 2001.
- 671 Jordanova, V. K., L. M. Kistler, J. U. Kozyra, G. V. Khazanov, and A. F. Nagy (1996),
672 Collisional losses of ring current ions, *J. Geophys. Res.*, *101*, 111.
- 673 Jordanova, V. K., J. U. Kozyra, G. V. Khazanov, A. F. Nagy, C. E. Rasmussen, and
674 M.-C. Fok (1994), A bounce-averaged kinetic model of the ring current ion
675 population, *Geophys. Res. Lett.*, *21*, 2785.
- 676 Jordanova, V. K., J. U. Kozyra, A. F. Nagy, and G. V. Khazanov (1997), Kinetic model
677 of the ring current-atmosphere interactions, *J. Geophys. Res.*, *102*, 14279.
- 678 Kennel, C. F., and H. E. Petschek (1966), Limit on stably trapped particle fluxes, *J.*
679 *Geophys. Res.*, *71*, 1.
- 680 Khazanov, G. V., K. V. Gamayunov, D. L. Gallagher, and J. U. Kozyra (2006), Self-
681 consistent model of magnetospheric ring current and propagating electromagnetic

- 682 ion cyclotron waves: Waves in multi ion magnetosphere, *J. Geophys. Res.*, *111*,
683 A10202, doi:10.1029/2006JA011833.
- 684 Khazanov, G. V., K. V. Gamayunov, D. L. Gallagher, J. U. Kozyra, and M. W. Liemohn
685 (2007), Self-consistent model of magnetospheric ring current and propagating
686 electromagnetic ion cyclotron waves. 2. Wave induced ring current precipitation
687 and thermal electron heating, *J. Geophys. Res.*, in press.
- 688 Khazanov, G. V., K. V. Gamayunov, and V. K. Jordanova, Self-consistent model
689 of magnetospheric ring current ions and electromagnetic ion cyclotron
690 waves: The 2–7 May 1998 storm (2003), *J. Geophys. Res.*, *108*, A12, 1419,
691 doi:10.1029/2003JA009856.
- 692 Khazanov, G. V., K. V. Gamayunov, V. K. Jordanova, and E. N. Krivorutsky (2002), A
693 self-consistent model of the interacting ring current ions and electromagnetic ion
694 cyclotron waves, initial results: Waves and precipitating fluxes, *J. Geophys. Res.*,
695 *107*, A6, 1085, doi:10.1029/2001JA000180.
- 696 Kozyra, J. U., T. E. Cravens, A. F. Nagy, E. G. Fontheim, and R. S. B. Ong (1984),
697 Effects of energetic heavy ions on electromagnetic ion cyclotron wave generation
698 in the plasmopause region, *J. Geophys. Res.*, *89*, 2217.
- 699 Kozyra, J. U., V. K. Jordanova, R. B. Horne, and R. M. Thorne (1997), Modeling of the
700 contribution of Electromagnetic Ion Cyclotron (EMIC) waves to stormtime ring
701 current erosion, in *Magnetic Storms, Geophys. Monogr. Ser.*, vol. 98, edited by
702 B. T. Tsurutani, W. D. Gonzalez, Y. Kamide, and J. K. Arballo, p. 187, AGU,
703 Washington, D. C..

- 704 LaBelle, J., R. A. Treumann, W. Baumjohann, G. Haerendel, N. Sckopke, G.
705 Paschmann, and H. Lühr (1988), The duskside plasmopause/ring current
706 interface: Convection and plasma wave observations, *J. Geophys. Res.*, *93*, 2573.
- 707 Lorentzen, K. R., M. P. McCarthy, G. K. Parks, J. E. Foat, R. M. Millan, D. M. Smith,
708 R. P. Lin, and J. P. Treilhou (2000), Precipitation of relativistic electrons by
709 interaction with electromagnetic ion cyclotron waves, *J. Geophys. Res.*, *105*,
710 5381.
- 711 Loto'aniu, T. M., B. J. Fraser, and C. L. Waters (2005), Propagation of electromagnetic
712 ion cyclotron wave energy in the magnetosphere, *J. Geophys. Res.*, *110*, A07214,
713 doi:10.1029/2004JA010816.
- 714 Loto'aniu, T. M., R. M. Thorne, B. J. Fraser, and D. Summers (2006), Estimating
715 relativistic electron pitch angle scattering rate using properties of the
716 electromagnetic ion cyclotron wave spectrum, *J. Geophys. Res.*, *111*, A04220,
717 doi:10.1029/2005JA011452.
- 718 Lyons, L. R., and R. M. Thorne (1972), Parasitic pitch angle diffusion of radiation belt
719 particles by ion cyclotron waves *J. Geophys. Res.*, *77*, 5608.
- 720 Lyons, L. R., and D. J. Williams (1984), *Quantitative Aspects of Magnetospheric*
721 *Physics*, D. Reidel, Dordrecht.
- 722 Mauk, B. H. (1982), Helium resonance and dispersion effects on geostationary Alfvén/ion
723 cyclotron waves, *J. Geophys. Res.*, *87*, 9107.
- 724 Meredith, N. P., R. M. Thorne, R. B. Horne, D. Summers, B. J. Fraser, and R. R.
725 Anderson (2003), Statistical analysis of relativistic electron energies for cyclotron

- 726 resonance with EMIC waves observed on CRRES, *J. Geophys. Res.*, *108*, A6,
727 1250, doi:10.1029/2002JA009700.
- 728 Rairden, R. L., L. A. Frank, and J. D. Craven (1986), Geocoronal imaging with
729 Dynamics Explorer, *J. Geophys. Res.*, *91*, 13613.
- 730 Rasmussen, C. E., S. M. Guiter, and S. G. Thomas (1993), Two-dimensional model of
731 the plasmasphere: Refilling time constants, *Planet. Space Sci.*, *41*, 35.
- 732 Rauch, J. L., and A. Roux (1982), Ray tracing of ULF waves in a multicomponent
733 magnetospheric plasma: Consequences for the general mechanism of Ion
734 Cyclotron Waves, *J. Geophys. Res.*, *87*, 8191.
- 735 Roux, A., S. Perraut, J. L. Rouch, C. de Villedary, G. Kremser, A. Korth, and D. T.
736 Young (1982), Wave-particle interactions near Ω_{He^+} observed on board GEOS 1
737 and 2: 2. Generation of ion cyclotron waves and heating of He^+ ions, *J. Geophys.*
738 *Res.*, *87*, 8174.
- 739 Sheldon, R. B., and D. C. Hamilton (1993), Ion transport and loss in the Earth's quiet
740 ring current, 1, Data and standard model, *J. Geophys. Res.*, *98*, 13491.
- 741 Soraas, F., K. Aarsnes, J. A. Lundblad, and D. S. Evans (1999), Enhanced pitch angle
742 scattering of protons at mid-latitudes during geomagnetic storms, *Phys. Chem.*
743 *Earth (C)*, *24*, 287.
- 744 Stern, D. P. (1975), The motion of a proton in the equatorial magnetosphere, *J.*
745 *Geophys. Res.*, *80*, 595.
- 746 Stix, T. H. (1992), *Waves in Plasmas*, Am. Inst. of Phys., College Park, Md.
- 747 Summers, D., and R. M. Thorne (2003), Relativistic electron pitch-angle scattering

- 748 by electromagnetic ion cyclotron waves during geomagnetic storms, *J. Geophys.*
749 *Res.*, *108*, A4, doi:10.1029/2002JA009489.
- 750 Thorne, R., and R. Horne (1994), Energy transfer between energetic ring current H^+
751 and O^+ by electromagnetic ion cyclotron waves, *J. Geophys. Res.*, *99*, 17275.
- 752 Thorne, R., and R. Horne (1997), Modulation of electromagnetic ion cyclotron instability
753 due to interaction with ring current O^+ during the geomagnetic storms, *J.*
754 *Geophys. Res.*, *102*, 14155.
- 755 Thorne, R. M., and C. F. Kennel (1971), Relativistic electron precipitation during
756 magnetic storm main phase, *J. Geophys. Res.*, *76*, 4446.
- 757 Volland, H. (1973), A semiempirical model of large-scale magnetospheric electric fields,
758 *J. Geophys. Res.*, *78*, 171.
- 759 Walt, M., and H. D. Voss (2001), Losses of ring current ions by strong pitch angle
760 scattering, *Geophys. Res. Lett.*, *28*, 3839.
- 761 Walt, M., and H. D. Voss (2004), Proton precipitation during magnetic storms
762 in August through November 1998, *J. Geophys. Res.*, *108*, A02201,
763 doi:10.1029/2003JA010083.
- 764 Yahnina, T. A., A. G. Yahnin, J. Kangas, J. Manninen, D. S. Evans, A. G. Demekhov,
765 V. Yu. Trakhtengerts, M. F. Thomsen, G. D. Reeves, and B. B. Gvozdevsky
766 (2003), Energetic particle counterparts for geomagnetic pulsations of Pc 1 and
767 IPDP types, *Annales Geophysicae*, *21*, 2281.
- 768 Young, D. T. (1983), Heavy ion plasmas in the outer magnetosphere, *J. Geophys. Res.*,
769 *52*, 167.

- 770 Young, D. T., H. Balsiger, and J. Geiss (1982), Correlations of magnetospheric ion
771 composition with geomagnetic and solar activity, *J. Geophys. Res.*, *87*, 9077.
- 772 Young D. T., T. J. Geiss, H. Balsiger, P. Eberhardt, A. Ghiedmetti, and H. Rosenbauer
773 (1977), Discovery of He^{2+} and O^{2+} ions of terrestrial origin in the outer
774 magnetosphere, *Geophys. Res. Lett.*, *4*, 561.
- 775 Young D. T., S. Perraut, A. Roux, C. de Villedary, R. Gendrin, A. Korth, G. Kremser,
776 and D. Jones (1981), Wave-particle interactions near Ω_{He^+} observed on GEOS 1
777 and 2: 1. Propagations of ion cyclotron waves in He^+ -rich plasma, *J. Geophys.*
778 *Res.*, *86*, 6755.
- 779 Zaharia, S., V. K. Jordanova, M. F. Thomsen, and G. D. Reeves (2006), Self-
780 consistent modeling of magnetic fields and plasmas in the inner magneto-
781 sphere: Application to a geomagnetic storm, *J. Geophys. Res.*, *111*, A11S14,
782 doi:10.1029/2006JA011619.

783 K. V. Gamayunov, National Space Science and Technology Center, NASA Marshall
784 Space Flight Center, Space Science Department, 320 Sparkman Drive, Huntsville, AL
785 35805, USA. (e-mail: konstantin.gamayunov@msfc.nasa.gov)

786 G. V. Khazanov, National Space Science and Technology Center, NASA Marshall
787 Space Flight Center, Space Science Department, 320 Sparkman Drive, Huntsville, AL
788 35805, USA. (e-mail: george.khazanov@msfc.nasa.gov)

789 Received _____

Figure 1. Equatorial plasma density distributions during the May 1998 event. The first row shows the cold electron plasma density distribution from the *Rasmussen et al.* [1993] model, and the second row provides a sum of cold plasma density and RC H^+ density as it follows from the simulation. The first, the second, and the third plasma sheet ion injections affect the total density distribution during 33–48, 58–68, and 78–90 hours, respectively. The specified hours are counted from 0000 UT on 1 May, 1998.

Figure 2. Simulated phase space distribution function for the RC H^+ . All the PSDFs are shown in the equatorial plane, and integrated over the entire solid angle. For each PSDFs, the first and the second numbers in parenthesis are the L-shell and MLT location, respectively. The corresponding RC proton temperature along the geomagnetic field line, T_{\parallel} , is calculated for the entire energy range. Note that there are the linear and logarithmic energy scales in the left-hand and right-hand boxes, respectively.

Figure 3. Equatorial growth/damping rates versus the wave normal angle for the He^{+} -mode of EMIC waves. The RC is assumed to be entirely made up of energetic protons, the thermal plasma consists of the cold electrons, and 77% of H^+ , 20% of He^+ , and 3% of O^+ , and the wave resonate interaction with thermal plasma is omitted. All the results are obtained for the wave frequency $\nu = \omega/2\pi = 0.475$ Hz, and taken from our global model at location L=5.25, MLT=15 ($B = 215.3$ nT), at 48 hours after 1 May 1998, 0000 UT. (a) The electron number density is also determined by the global model, and $n_e = n_0 = 68.3 \text{ cm}^{-3}$ (nominal case). In order to produce the results (b), (c), and (d), we keep all parameters the same, except the electron number densities $n_e = 1.2 \times n_0$, $n_e = 1.5 \times n_0$, and $n_e = 2 \times n_0$ are respectively adopted.

Figure 4. Snapshots of the equatorial (MLT, L-shell) distributions of squared wave magnetic field for the He^+ -mode. The results are obtained by solving equations (1) and (2) along with the ray tracing equations. The first row corresponds to the case when the RC ions are only treated as a source of free energy to generate waves, and omitted in the real part of the wave dispersion relation. The second row demonstrates distribution when the RC ions are taken into account in both the real and imaginary parts of the wave dispersion relation. In both cases, the total ion composition is assumed to be 77% of H^+ , 20% of He^+ , and 3% of O^+ through an entire simulation domain.

793

Figure 5. The RC proton precipitating fluxes averaged over the equatorial pitch-angle loss cone and integrated over the energy range 1 – 50 keV. The first row represents the results without the RC ions in the real part of the EMIC wave dispersion relation. The second row shows precipitation in a case when the RC ions are taken into account in both the real and imaginary parts of the wave dispersion relation.

794

May 2-7, 1998: Thermal and
Sum of Thermal and RC Plasma Densities

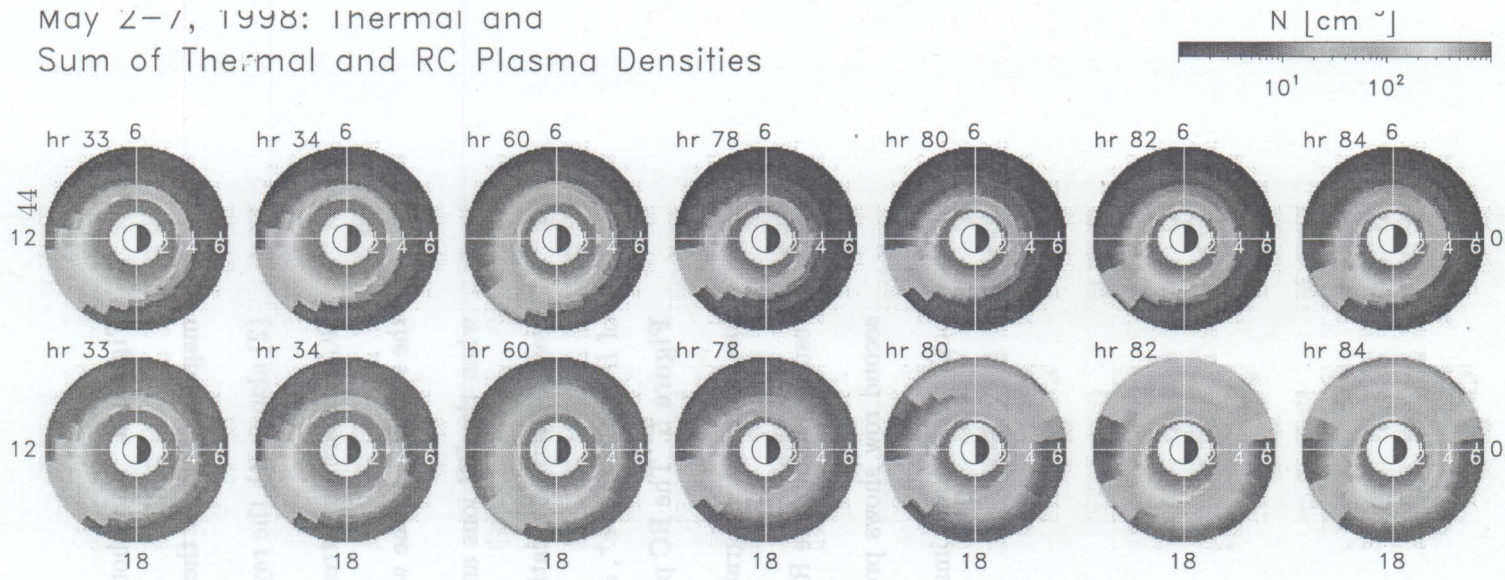


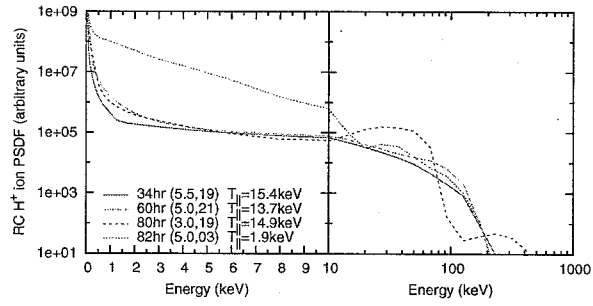
Figure 1.

798

796

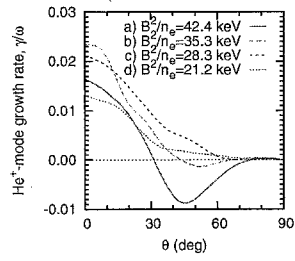
797

795



799

800 **Figure 2.**



801

802 **Figure 3.**

May 2-7, 1998: B-field Spectrogram (W/Kay)
 Without and With RC Ions in Dispersion Relation

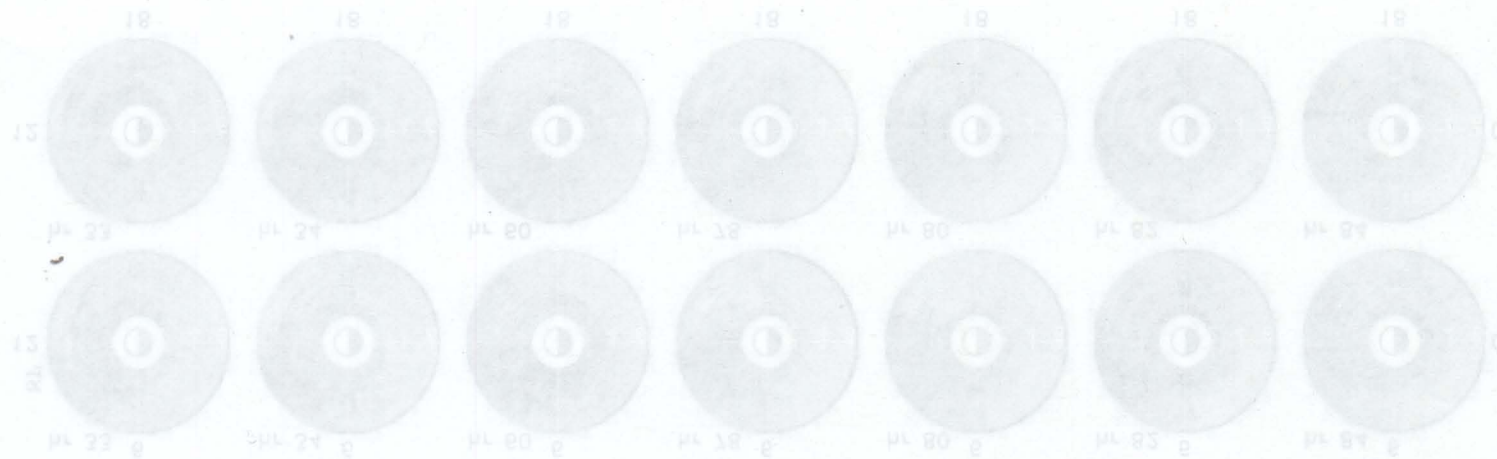
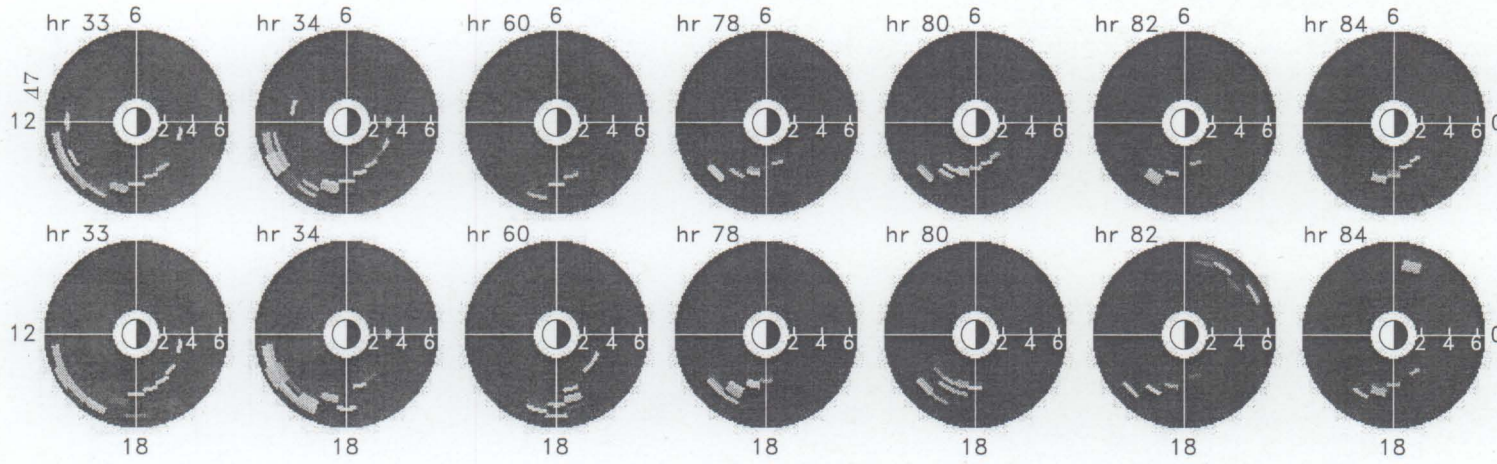
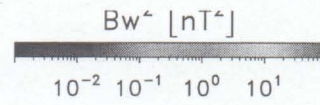
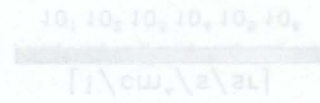


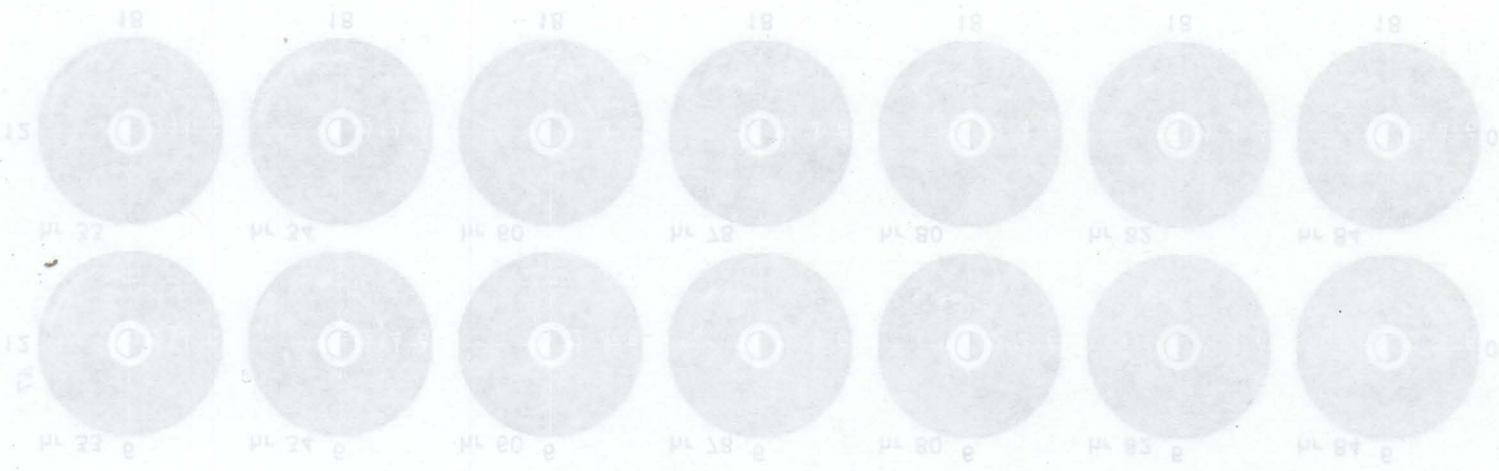
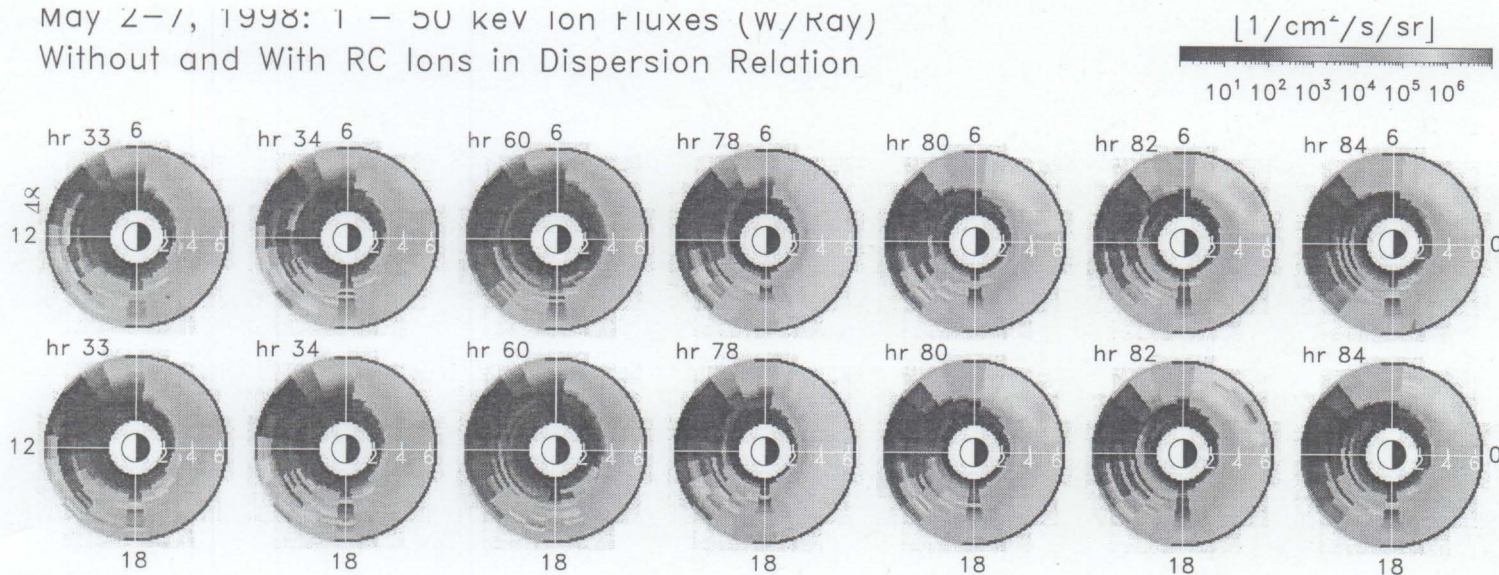
Figure 4.

806
804
805

Without and with RC ions in dispersion relation
 May 2-7, 1998: 1 - 20 kHz ion fluxes (W/Kay)



May 2-7, 1998: 1 - 50 keV Ion Fluxes (W/Ray)
 Without and With RC Ions in Dispersion Relation



810 Figure 5.

808

809

Without and With RC ions in dispersion relation
 May 2-7, 1998: 1-50 keV ion fluxes (W/Ray)

